ORIGINAL RESEARCH

Entropy generation analysis on zero mass flux effects of nonlinear mixed convective Williamson nanofluid flow with christov-Cattaneo heat flux

D. Mahalakshmi¹ · B. Vennila¹ · K. Loganathan²

Abstract

The passage of non-Newtonian fluids across the stretching plate exerts a significant impact and finds applications in various industrial sectors, such as fluidics networks, fluid agitation, thermal reactors, liquid chromatography, semiconductors, tissue regeneration, and gene delivery to organs. In this study, we investigated the hydrodynamic Williamson nanofluid flow over a stretchy surface with zero mass flux, Christov–Cattaneo (C–C) theory, non-linear mixed convection, and passive controls of nanomaterials. Thermophoresis and Brownian motion impressions are also taken in the present flow. The second law of thermodynamics is also used to determine the entropy generation. By using the proper similarity alterations, the PDEs (governing equations) are converted into non-linear ODEs. To crack the non-linear ODEs, the homotopy analysis method is used. There is a detailed discussion of the effects of magnetic, Weissenberg, radiation, Brownian motion, the Bejan parameter, and the entropy creation of various factors. Additionally, the heat, mass transfer rate, and skin friction are assessed. Also, compare skin friction and the Nusselt number with previous studies. The Weissenberg number and Brinkman parameter shows the opposite tendency in entropy generation and Bejan number profiles.

Keywords Williamson nanofluid · Christov–Cattaneo model · Nonlinear mixed convection · Entropy creation · Homotopy analysis method

✉ B. Vennila
vennilab@srmist.edu.in

1. Department of Mathematics, SRM Institute of Science and Technology, SRM Nagar, Kattankulathur, Chengalpattu 603203, Tamil Nadu, India

2. Department of Mathematics and Statistics, Manipal University Jaipur, Jaipur 303007, Rajasthan, India

List of symbols

$\hat{a}$	Stretchy rate $\left(\text{s}^{-1}\right)$
Bi	Biot parameter
Be	Bejan parameter
Br	Brinkman parameter
B_0	Constant magnetic field $\left(\text{kgs}^{=2}\text{A}^{-1}\right)$
C	Concentration $\left(\text{kgm}^{-3}\right)$
Cr	Reaction rate number
c_p	Specific heat at constant pressure $\left(\text{J kg}^{-1}\text{K}^{-1}\right)$
C_∞	Free stream concentration $\left(\text{kgm}^{-3}\right)$
C_w	Fluid concentration at wall $\left(\text{kgm}^{-3}\right)$
C_f	Skin-friction coefficient
D_B and D_T	Brownian and Thermophoresis diffusion coefficients $\left(\text{m}^2\text{s}^{-1}\right)$
E_G	Entropy creation number
Ec	Eckert parameter
$f(\eta)$	Velocity similarity function
f_w	Suction/blowing parameter
h_f	Convective heat transmission coefficient $\left(\text{Wm}^{-1}\text{K}^{-1}\right)$
k	Thermal conductivity $\left(\text{Wm}^{-1}\text{K}^{-1}\right)$
Le	Lewis number
M	Hartmann parameter
Nb	Brownian motion number
Nt	Thermophoresis number
Nu	Nusselt parameter
N^*	Ratio of concentration to thermal buoyancy forces
Pr	Prandtl number
Q_0	Heat source/sink coefficient
$\hat{q}$	Heat flux $\left(\text{Wm}^{-2}\right)$
Rd	Radiation number
Re	Reynolds parameter
Sh	Sherwood parameter
S	Heat source parameter
T	Temperature (K)
T_∞	Free stream temperature (K)
T_f	Convective surface temperature (K)
$\hat{u}_\text{w}$	Sheet velocity $\left(\text{ms}^{-1}\right)$
$\hat{u}, \hat{v}$	Velocity apparatuses in $\left(\widehat{x}, \hat{y}\right)$ axes $\left(\text{ms}^{-1}\right)$
$\hat{v}_\text{w} > 0$	Suction velocity
$\hat{v}_\text{w} < 0$	Blowing velocity
We	Weissenberg number
$\widehat{x}, \hat{y}$	Cartesian coordinates (m)
PDEs	Partial differential equations
ODEs	Ordinary differential systems
C–C	Christov–Cattaneo heat flux

Greeks

β	Relaxation time
β_t	Nonlinear mixed convection temperature component
β_C	Nonlinear mixed convection concentration component
$\phi(\eta)$ and $\theta(\eta)$	Concentration and tedmperature similarity functions
Γ	Non-dimensional velocity slip parameter
γ	Non-dimensional thermal relaxation time
η	Similarity parameter
λ_T	Thermal relaxation time
λ	Non-dimensional immovable
ν	Kinematic viscosity $\left(\mathrm{m^2 s^{-1}}\right)$
Ω	Non-dimensional temperature variance
τ	Ratio of the effective heat capacity
ρ	Density $\left(\mathrm{kgm^{-1}}\right)$
σ	Electrical conductance variable (Sm)
ψ	Stream function $\left(\mathrm{ms^{-1}}\right)$
ζ	Non-dimensional concentration variance

1 Introduction

Considering its significance in engineering and business, the investigation of heat and mass transference is a particularly significant subject for researchers. It is used in biomedical and manufacturing processes, together with food preparation and tissue conduction. Because of the many applications of non-Newtonian fluids, investigators have expressed a strong interest in studying them. The main reason for this is the prevalence of these fluids in nature. Non-Newtonian performance is widely employed in industries like mining, where slurries and muck are regularly controlled, and in services like lubricating and biomedical flows. Although non-Newtonian fluids have been the subject of a sizable amount of research, non-Newtonian fluid models still need a great deal of work. Williamson fluid is classified as a non-Newtonian fluid having shear-thinning characteristics, meaning that its viscosity gets thinner as shear stress intensity rises.

Nanofluids have emerged as one of the most sought-after research fields due to their low heat resistance and efficient thermal properties. In addition, it's crucial to maintain the chilling of technical items like CPUs, laptops, power electronics, engines, and high-powered emissions in order for them to operate as intended. Choi [1] studied the thermal conductivity's properties of different types of nanofluids. Kuznetsov and Nield [2] inspected a study on a vertical plate of natural convection boundary layer nanofluid flow. Khan and Pop [3] discussed fluid flow with nanomaterials over an extending surface. Haddad et al. [4] inspected the impressions of thermophoresis and the Brownian of nanofluid flow. A study on a stretchy sheet of Williamson fluid flow with nanomaterials was discussed by Nadeem et al. [5]. Khan et al. [6] inspected the Oldroyd-B fluid flow with the impacts of motile organisms and the active Prandtl

approach. Bilal et al. [7] elucidate the flow characteristics of the Non-Newtonian Carreau fluid model within a square chamber. The Carreau fluid model describes the relationship between stress and strain for a non-elastic material, considering both infinite and zero stress magnitudes. Bilal et al. [8] investigate the physical properties of Carreau nanofluid on a linearly extensible cylinder, as well as its potential application in bioconvection phenomenon.

Fourier's law [9] also revealed the heat transfer mechanism in 1822. This law serves as the foundation for the hypothesis that the mode under investigation may detect the actual temperature quickly. Cattaneo [10] corrected this problem by adding a thermal relaxation time to Fourier's law. This expression denotes the amount of time required for a mode to transfer heat to the nearby elements. Christov [11] improved this model as well. The innovative model (C–C) is recognized as the Cattaneo-Christov heat flow model. The C–C model and the second-order slip, reaction rate, and double diffusion impacts on hydromagnetic convective Oldroyd-B liquid flow approaching an extensible surface were examined by Loganathan et al. [12]. Imtiaz et al. [13] inspected the fluid flow and heat transference impact of third-grade fluid in the presence of C–C models and reaction rates. Ramadevi et al. [14] inspected the hydromagnetic mixed convection micropolar fluid flow over a stretchy surface using a modified Fourier's heat flux model. The impressions of heat transference and entropy creation of time-dependent MHD fluid flow over a stretchy revolving disk solved via an artificial neural system and particle swarm optimization procedure were discussed by Rashidi et al. [15]. Khan and Alzahrani [16] conducted a study on the flow of a non-Newtonian nanofluid (specifically, the Jeffrey fluid) towards a stretched surface, focusing on the Cattaneo-Christov double diffusion. López et al. [17] analyzed the entropy creation and non-linear thermal radiation impacts of hydromagnetic fluid flow with nanomaterials over a porous, erect microchannel. Khan et al. [18] considered the non-linear mixed convective nanofluid flow to analyze the entropy creation in the existence of Joule heating and slipping situations. Qing et al. [19] inspected the entropy creation study of hydromagnetic Casson fluid flow with nanomaterials over a porous extending or reducing surface. Sheikholeslami and Ganji [20] discussed the MHD nanofluid flow to optimize the entropy creation solved via the Lattice Boltzmann method. Liao and Tan [21] discussed a generic approach to searching out the series outcomes of non-linear PDEs.

The classification of the elements that cause the loss of useful energy makes the entropy computation of flow and heat transfer systems crucial. Energy loss may jeopardize the thermally designed system's efficiency. Reducing the entropy-producing variables can increase the system's output. Loganathan et al. [22] inspected the Williamson nanofluid flow over a slipping stretchy surface to control the passive situation of nanomaterials. Khan and Alzahrani [23] investigated the phenomenon of nonlinear mixed convection in a dissipative convective flow of micropolar fluid towards a stretched surface. Mixed convection refers to the simultaneous occurrence of forced and natural convection mechanisms. Eswaramoorthi et al. [24] discussed the double diffusion and chemical reaction impact of a radiative visco-elastic fluid flow over a stretchy surface. Aquino and Bo-ot [25] investigated the Homotopy analysis scheme to address the two-level set of equations and provide conclusions that would

identify turbulent activity. The study conducted by Chu et al. [26] focuses on ana-lyzing the entropy production in an inclined channel that is filled with Rabinowitsch fluid. Hayat et al. [27] discussed the radiative third-grade fluid flow over a radiative surface with Joule heating impact. Ghasemi et al. [28] inspected the hydromagnetic blood nanofluid flow that passes through porous arteries. Wang [29] discussed the natural convection fluid flow over an erect, stretchy surface. Reddy and Sidawi [30] studied the suction and blowing impacts on the erect stretchy surface of natural con-vection fluid flow. Khan and Pop [31] considered a boundary layer fluid flow with nanomaterials over a stretchy surface. Makinde and Aziz [32] inspected the convec-tive boundary layer fluid flow with nanomaterials over a stretchy surface. Gorla and Gireesha [33] studied the dual results for Williamson fluid flow with nanomaterials over a stretchy/shrinking sheet and stagnation point.

As far as we know, no research has been done on how entropy building with C–C and zero mass flux affects the MHD 2D non-linear mixed convection flow of a Williamson nano-liquid caused by a stretchable surface. There are still few studies involving the C–C heat flux and entropy creation. Although there are a number of techniques for studying extremely non-linear equations, the homotopy analysis scheme is considered to be the best. The goal of the current essay is to mathematically formulate such flows with the help of the HAM approach. Upon completing our investigation, we furnish the solutions to the subsequent inquiries for additional research:

- How the non-linear mixed convection affects the flow rate?
- What are the impacts of embedded variables on entropy and Bejan number profile like Weissenberg number, Eckert number, and Brinkman number?
- How thermos phoresies and Brownian motion affects the nanoparticle concentra-tion?

2 Flow analysis

The current study enclosed with time-independent 2-D flow of incompressible, viscid and radiative Williamson fluid with nanomaterials over a flat stretchy surface. The bottom of the plate induces the convective heating temperature T_f. The perpendicular direction of the plate is subjected to the imposition of a uniform transverse magnetic field B_0. Assume that $\hat{u} = \hat{u}_w = \hat{a}\hat{x}$ is the stretchy velocity and that $'\hat{a}\prime$ is the stretching rate. While the $\hat{y}$-track is moving vertically, the $\hat{x}$-track is stretched out. Nadeem et al. [5] present the Williamson fluid Cauchy stress tensor.

$$\delta = -pI + \Phi \tag{1}$$

$$\Phi = \left(\mu_\infty + \frac{\mu_0 - \mu_\infty}{1 - \beta\alpha} \right)\varepsilon \tag{2}$$

where Φ, μ_0, μ_∞ is the extra stress tensor, viscosities at zero and endless shear stresses, respectively, time invariable is defining as $\beta > 0$ i, ε is the initial Rivilin-Erickson

tensor and shear rate α is stated as

$$\alpha = \sqrt{\frac{1}{2}\pi \cdot \pi} = trace\left(\varepsilon^2\right) \tag{3}$$

After Gorla and Gireesha [33], we have researched

$$M_\infty = 0, \ \beta\alpha < 1. \tag{4}$$

So, we obtain

$$\Phi = \left(\frac{\mu_0}{1 - \beta\alpha}\right)\varepsilon \tag{5}$$

otherwise using binomial expansion

$$\Phi = \mu_0(1 + \beta\alpha)\varepsilon \tag{6}$$

$$A = \left[\left(\frac{\partial\hat{u}}{\partial\hat{x}}\right)^2 + \left(\frac{\partial\hat{u}}{\partial\hat{y}}\right)^2 + \frac{1}{2}\left(\frac{\partial\hat{v}}{\partial\hat{x}} + \frac{\partial\hat{u}}{\partial\hat{y}}\right)^2\right]^{\frac{1}{2}} \tag{7}$$

$$\Phi_{\hat{x}\hat{x}} = 2\mu_0(1 + \beta\alpha)\frac{\partial\hat{u}}{\partial\hat{x}} \tag{8}$$

$$\Phi_{\hat{x}\hat{y}} = \Phi_{\hat{y}\hat{x}} = \mu_0(1 + \beta\alpha)\left(\frac{\partial\hat{v}}{\partial\hat{x}} + \frac{\partial\hat{u}}{\partial\hat{y}}\right) \tag{9}$$

$$\Phi_{\hat{y}\hat{y}} = 2\mu_0(1 + \beta\alpha)\frac{\partial\hat{v}}{\partial\hat{y}} \tag{10}$$

Figure 1 displays a physical structure of the model construction.
The governing flow equations are [22]:

$$\frac{\partial\hat{u}}{\partial\hat{x}} + \frac{\partial\hat{v}}{\partial\hat{y}} = 0 \tag{11}$$

$$\hat{u}\frac{\partial\hat{u}}{\partial\hat{x}} + \hat{v}\frac{\partial\hat{u}}{\partial\hat{y}} = \nu\frac{\partial^2\hat{u}}{\partial\hat{y}^2} + \sqrt{2}\nu\beta\frac{\partial\hat{u}}{\partial\hat{y}}\frac{\partial^2\hat{u}}{\partial\hat{y}^2} - \frac{\sigma B_0^2}{\rho}\hat{u} + \frac{g}{\rho}\left(\lambda_1(T - T_\infty) + \lambda_2\left((T - T_\infty)^2\right)\right)$$
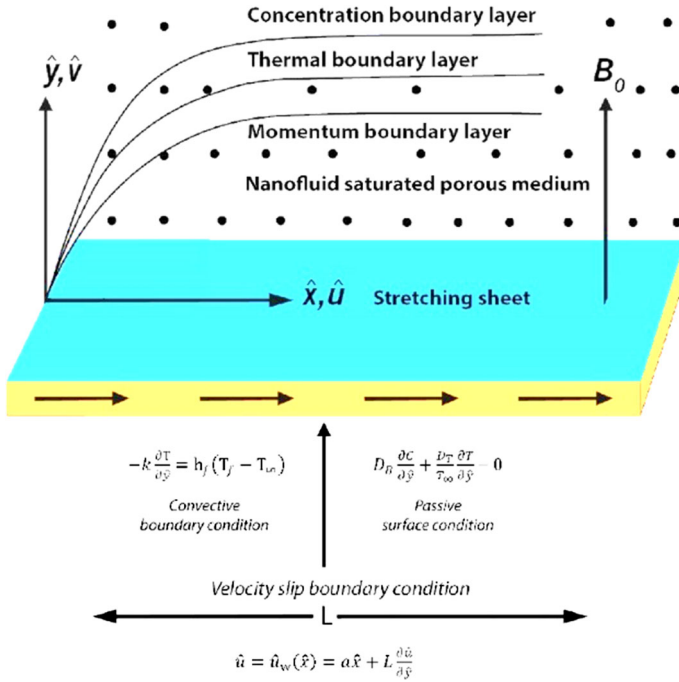$$+ \frac{g}{\rho}\left(\lambda_3(C - C_\infty) + \lambda_4\left((C - C_\infty)^2\right)\right) \tag{12}$$

Fig. 1 Flow diagram

$$\hat{u}\frac{\partial T}{\partial \hat{x}} + \hat{v}\frac{\partial T}{\partial \hat{y}} = \frac{k}{\rho c_p}\frac{\partial^2 T}{\partial \hat{y}^2} - \frac{1}{\rho c_p}\frac{\partial q_r}{\partial \hat{y}} + \frac{Q_0}{\rho c_p}(T - T_\infty)$$

$$+ \tau\left[D_B\frac{\partial C}{\partial \hat{y}}\frac{\partial T}{\partial \hat{y}} + \frac{D_T}{T_\infty}\left(\frac{\partial T}{\partial \hat{y}}\right)^2\right]$$

$$+ \frac{\sigma B_0^2}{\rho c_p}\hat{u}^2 + \frac{\mu_0}{\rho c_p}\left(\frac{\partial \hat{u}}{\partial \hat{y}}\right)^2 + \frac{\mu_0}{\rho c_p}\beta\left(\frac{\partial \hat{u}}{\partial \hat{y}}\right)^3 \tag{13}$$

$$\hat{u}\frac{\partial C}{\partial \hat{x}} + \hat{v}\frac{\partial C}{\partial \hat{y}} = D_B\frac{\partial^2 C}{\partial \hat{y}^2} + \frac{D_T}{T_\infty}\frac{\partial^2 T}{\partial \hat{y}^2} - k_m(C - C_\infty) \tag{14}$$

$$\hat{u} = \hat{u}_w(\hat{x}) = \hat{a}\hat{x} + L\frac{\partial \hat{u}}{\partial \hat{y}}, \ \hat{v} = \hat{v}_w, \ -k\frac{\partial T}{\partial \hat{y}} = h_f(T_f - T_\infty),$$

$$D_B\frac{\partial C}{\partial \hat{y}} + \frac{D_T}{T_\infty}\frac{\partial T}{\partial \hat{y}} = 0 \text{ at } \hat{y} = 0$$

$$\hat{u} \to 0, \ T \to T_\infty, \ C \to C_\infty \text{ as } \hat{y} \to \infty \tag{15}$$

The heat flux $\hat{q}$ is provided by [10, 11].

$$\hat{q} + \lambda_T \left(\frac{\partial \hat{q}}{\partial t} + \left(\mathbb{V} \cdot \nabla \hat{q} - \hat{q} \cdot \nabla \mathbb{V} \right) + (\nabla \cdot \mathbb{V})\hat{q} \right) = -k\nabla T \tag{16}$$

For $\lambda_T = 0$, Eq. (16) reduces to Fourier's law. The necessity for incompressible fluids is $\nabla \cdot \mathbb{V} = 0$ and we achieve,

$$\hat{q} + \lambda_T \left(\frac{\partial \hat{q}}{\partial t} + \left(\mathbb{V} \cdot \nabla \hat{q} - \hat{q} \cdot \nabla \mathbb{V} \right) \right) = -k\nabla T \tag{17}$$

Removing $\hat{q}$ between Eqns. (13) and (17), we arrive at the subsequent energy equation

$$\begin{aligned}
&\hat{u}\frac{\partial T}{\partial \hat{x}} + \hat{v}\frac{\partial T}{\partial \hat{y}} + \lambda_T \left(\hat{u}^2 \frac{\partial^2 T}{\partial \hat{x}^2} + \hat{v}^2 \frac{\partial^2 T}{\partial \hat{y}^2} + \left(\hat{u}\frac{\partial \hat{u}}{\partial \hat{x}}\frac{\partial T}{\partial \hat{x}} + \hat{v}\frac{\partial \hat{u}}{\partial \hat{y}}\frac{\partial T}{\partial \hat{x}} \right) + 2\hat{u}\hat{v}\frac{\partial T^2}{\partial \hat{x}\partial \hat{y}} \right) \\
&+ \left(\hat{u}\frac{\partial \hat{v}}{\partial \hat{x}}\frac{\partial T}{\partial \hat{y}} + \hat{v}\frac{\partial \hat{v}}{\partial \hat{y}}\frac{\partial T}{\partial \hat{y}} \right) = \frac{k}{\rho c_p}\frac{\partial^2 T}{\partial \hat{y}^2} - \frac{1}{\rho c_p}\frac{\partial q_r}{\partial \hat{y}} + \frac{Q_0}{\rho c_p}(T - T_\infty) \\
&+ \tau \left[D_B \frac{\partial C}{\partial \hat{y}}\frac{\partial T}{\partial \hat{y}} + \frac{D_T}{T_\infty}\left(\frac{\partial T}{\partial \hat{y}}\right)^2 \right] + \frac{\sigma B_0^2}{\rho c_p}\hat{u}^2 + \frac{\mu_0}{\rho c_p}\left(\frac{\partial \hat{u}}{\partial \hat{y}}\right)^2 + \frac{\mu_0}{\rho c_p}\beta\left(\frac{\partial \hat{u}}{\partial \hat{y}}\right)^3
\end{aligned} \tag{18}$$

The transformations are [22],

$$\psi = \sqrt{\hat{a}v}\hat{x}f(\eta), \ \hat{u} = \frac{\partial \psi}{\partial \hat{y}}, \ \hat{v} = -\frac{\partial \psi}{\partial \hat{x}}, \ \eta = \sqrt{\frac{\hat{a}}{v}}\hat{y}, \ \hat{v} = -\sqrt{\hat{a}v}f(\eta), \ \hat{u} = \hat{a}\hat{x}f'(\eta)$$

$$\theta(\eta) = \frac{T - T_\infty}{T_f - T_\infty}, \ \phi(\eta) = \frac{C - C_\infty}{C_\infty}. \tag{19}$$

We have,

$$f''' + Wef''f''' - f'^2 + ff'' - Mf' + \lambda\theta(1 + \beta_t\theta) + \lambda\phi N^*(1 + \beta_c\phi) = 0 \tag{20}$$

$$\begin{aligned}
&\theta'' + Rd\left((\theta(\theta_w - 1) + 1)\right)^2 \left(3\theta'^2(\theta_w - 1) + (\theta(\theta_w - 1) + 1)\theta''\right) \\
&+ Prf\theta' + PrS\theta - Pr\gamma\left(f^2\theta'' + ff'\theta'\right) + Pr\left(Nb\theta'\phi' + Nt\theta'^2\right) \\
&+ Pr\left(MEcf'^2 + Ecf''^2 + \frac{We}{\sqrt{2}}Ecf''^3\right) = 0
\end{aligned} \tag{21}$$

$$\phi'' + Lef\phi' + \frac{Nt}{Nb}\theta'' - LeCr\phi = 0 \tag{22}$$

with limitations $f(0) = f_w$, $f\prime(0) = 1 + \Gamma\frac{We}{\sqrt{2}}f''(0)$, $\theta'(0) = -Bi(1 - \theta(0))$, $Nb\phi'(0) + Nt\theta'(0) = 1$

$$f'(\eta) \to 0, \, \theta(\eta) \to 0, \, \phi(\eta) \to 0 \text{ as } \eta \to \infty \tag{23}$$

The variables are stated as $We = \sqrt{\frac{2\hat{a}^3}{\upsilon}}\beta\hat{x}$, $\Gamma = L\sqrt{\frac{\hat{a}}{\nu}}$, $M = \sigma B_0^2/\rho\hat{a}$, $Pr = \rho c_p/k$, $Ec = \frac{\hat{a}^2\hat{x}^2}{c_p(T_f - T_\infty)}$, $Rd = (4\sigma^* T_\infty^3)/(kk^*)$, $S = \frac{Q_0}{\rho c_p}$, $\gamma = \lambda_T a$, $Bi = \frac{h_f}{k}\sqrt{\nu/\hat{a}}$, $Nb = \frac{\tau D_B}{\nu}C_\infty$, $Nt = \frac{\tau D_T}{\nu}(T_f - T_\infty)$, $Cr = \frac{k_m}{a}$. $\beta_t = \frac{\lambda_2(T_f - T_\infty)}{\lambda_2}$, $\beta_C = \frac{\lambda_4(C_\infty)}{\lambda_3}$.

The following physical quantities are those of relevance to engineers:

$$C_f Re^{0.5} = \left[f''(0) + f''^2\frac{We}{2}(0)\right] \tag{24}$$

$$Nu Re^{-0.5} == -\left(1 + \frac{3}{4}Rd\left((\theta_w - 1)(\theta(0))^3\right)\right)\theta'(0) \tag{25}$$

In zero mass flux state, the local Sherwood number turns identically zero, as demonstrated in [22]:

$$Sh Re^{-0.5} = \frac{Nt}{Nb}\theta'(0) \tag{26}$$

3 Formulation of entropy generation

The entropy creation is stated as

$$S'''_{gen} = \frac{K_0}{T_\infty^2}\left[\left(\frac{\partial T}{\partial \hat{x}}\right)^2 + \left(\frac{\partial T}{\partial \hat{y}}\right)^2 + \frac{16\sigma^* T_\infty^3}{3kk^*}\left(\frac{\partial T}{\partial \hat{y}}\right)^2\right] + \frac{\mu}{T_\infty}\left[\left(\frac{\partial \hat{u}}{\partial \hat{y}}\right)^2 + \beta\left(\frac{\partial \hat{u}}{\partial \hat{y}}\right)^3\right]$$
$$+ \left[\frac{\partial \hat{u}}{\partial \hat{y}} + \frac{\partial \hat{v}}{\partial \hat{x}}\right]^2 + \frac{RD}{C_\infty}\left[\left(\frac{\partial C}{\partial \hat{y}}\right)^2\right] + \frac{RD}{T_\infty}\left[\left(\frac{\partial T}{\partial \hat{y}}\right)\left(\frac{\partial C}{\partial \hat{y}}\right)\right] + \frac{\sigma B_0^2}{T_\infty}\hat{u}^2 + \frac{\nu}{k_p}\hat{u}^2 \tag{27}$$

$$N_T = \frac{K_0}{T_\infty^2}\left[\left(\frac{\partial T}{\partial \hat{y}}\right)^2 + \frac{16\sigma^* T_\infty^3}{3kk^*}\left(\frac{\partial T}{\partial \hat{y}}\right)^2\right]$$
$$= \text{Contribution of entropy due to thermal transfer.}$$

$$N_f = \frac{\mu}{T_\infty}\left[\left(\frac{\partial \hat{u}}{\partial \hat{y}}\right)^2 + \beta\left(\frac{\partial \hat{u}}{\partial \hat{y}}\right)^3\right] = \text{Contribution of entropy due to fluid friction.}$$

$$N_C = \frac{RD}{C_\infty}\left(\frac{\partial C}{\partial \hat{y}}\right)^2 + \frac{RD}{T_\infty}\left(\frac{\partial T}{\partial \hat{y}}\right)\left(\frac{\partial C}{\partial \hat{y}}\right)$$
$$= \text{Contribution of entropy due to mass transfer.}$$

$$N_m = \left(\frac{\sigma B_0^2}{T_\infty} + \frac{\nu}{k_p}\right)\hat{u}^2$$
$$= \text{Contribution of entropy due to magnetic field and porous medium.}$$

where the following is a description of the characteristic entropy generation rate S_0''' :

$$S_0''' = \frac{K_0}{T_\infty^2}\frac{(\Delta T)^2}{l^2}$$

As a result, the following is the value of the non-dimensional entropy creation number:

$$E_G = \frac{S_{gen}'''}{S_0'''}$$

$$E_G = Re\left(1 + Rd\left(1 + (\theta\,(\theta_w - 1) + 1)^2\right)\right)\theta'^2 + Re\frac{Br}{\Omega}\left(f''^2 + \frac{We}{\sqrt{2}}f''^3\right)$$
$$+ Re\left(\frac{\zeta}{\Omega}\right)^2 \lambda\phi'^2 + Re\frac{\zeta}{\Omega}\lambda\phi'\theta' + \frac{Br}{\Omega}Mf'^2 \tag{28}$$

Bejan number is written as

$$Be = \frac{\text{Entropy creation due to heat and mass transmission}}{\text{Total entropy creation}} \tag{29}$$

$$Be = \frac{Re\left(1 + Rd\left(1 + (\theta(\theta_w - 1) + 1)^2\right)\right)\theta'^2 + Re\left(\frac{\zeta}{\Omega}\right)^2\lambda\phi'^2 + Re\frac{\zeta}{\Omega}\lambda\phi'\theta'}{Re\left(1 + \frac{4}{3}Rd\right)\theta'^2 + Re\frac{Br}{\Omega}\left(f''^2 + \frac{We}{\sqrt{2}}f''^3\right) + Re\left(\frac{\zeta}{\Omega}\right)^2\lambda\phi'^2 + Re\frac{\zeta}{\Omega}\lambda\phi'\theta' + \frac{Br}{\Omega}(M + K_P)f'^2} \tag{30}$$

4 HAM solutions

The main hypotheses for the homotopy process are described as

$$f_0 = f_w + \left(\frac{1}{1+\Gamma}\right)1 - e^{-\eta}, \; \theta_0 = \frac{Bi*e^{-\eta}}{1+Bi} \; \text{and} \; \phi_0 = -\left(\frac{Nt}{Nb}\right)*\frac{Bi*e^{-\eta}}{1+Bi} \tag{31}$$

The auxiliary linear operators L_f, L_θ and L_ϕ are obtained as

$$L_f = f'''(\eta) - f'(\eta), \ L_\theta = \theta''(\eta) - \theta(\eta) \text{ and } L_\phi = \phi''(\eta) - \phi(\eta) \tag{32}$$

The above linear operators satisfying

$$\mathcal{L}_f\left[A_1 + A_2 e^\eta + A_3 e^{-\eta}\right] = 0, \ \mathcal{L}_\theta\left[A_4 e^\eta + A_5 e^{-\eta}\right] = 0 \text{ and } \mathcal{L}_\phi\left[A_6 e^\eta + A_7 e^{-\eta}\right] = 0 \tag{33}$$

here $A_j(j = 1 - 7)$ denote the licentious conditions.

Zero[th] order deformation:

$$(1 - p)\mathcal{L}_f[f(\eta; p) - f(\eta)] = ph_f \mathcal{N}_f[f(\eta; p)] \tag{34}$$

$$(1 - p)\mathcal{L}_\theta[\theta(\eta; p) - \theta_0(\eta)] = ph_\theta \mathcal{N}_\theta[\theta(\eta; p), \ f(\eta; p), \ \phi(\eta; p)] \tag{35}$$

$$(1 - p)\mathcal{L}_\phi[\phi(\eta; p) - \phi_0(\eta)] = ph_\phi \mathcal{N}_\phi[\phi(\eta; p), \ \theta(\eta; p), \ f(\eta; p)] \tag{36}$$

where $p\varepsilon[0, 1]$ and h_f, h_θ and h_ϕ are the non-zero auxiliary constants and $\mathcal{N}_f$, $\mathcal{N}_\theta$ and $\mathcal{N}_\phi$ are the nonlinear operators given by

$$\begin{aligned}
\mathcal{N}_f\left[f(\eta; p), \theta(\eta; p)\right] = & \frac{\partial^3 f(\eta; p)}{\partial \eta^3} + We \frac{\partial^2 f(\eta; p)}{\partial \eta^2} \frac{\partial^3 f(\eta; p)}{\partial \eta^3} \\
& + f(\eta; p) \frac{\partial^2 f(\eta; p)}{\partial \eta^2} - M \frac{\partial f(\eta; p)}{\partial \eta} \\
& + \lambda \theta(\eta; p)(1 + \beta_t \theta(\eta; p)) + \lambda \phi(\eta; p) N^*(1 + \beta_c \phi(\eta; p))
\end{aligned} \tag{37}$$

$$\mathcal{N}_\theta[f(\eta; p), \theta(\eta; p), \phi(\eta; p)]$$

$$\begin{aligned}
= & \frac{\partial^2 \theta(\eta; p)}{\partial \eta^2} + Rd((\theta(\eta; p)(\theta_w - 1) + 1))^2 \left(3\left(\frac{\partial \theta(\eta; p)}{\partial \eta}\right)^2 (\theta_w - 1) + (\theta(\eta; p)(\theta_w - 1) + 1) \frac{\partial^2 \theta(\eta; p)}{\partial \eta^2}\right) \\
& + \Pr f(\eta; p) \frac{\partial \theta(\eta; p)}{\partial \eta} + S\theta(\eta; p) - \Pr \gamma[[f(\eta; p)]^2 \frac{\partial^2 \theta(\eta; p)}{\partial \eta^2} - \Pr \gamma f(\eta; p) \frac{\partial f(\eta; p)}{\partial \eta} \frac{\partial \theta(\eta; p)}{\partial \eta} \\
& + \Pr Nb \frac{\partial \theta(\eta; p)}{\partial \eta} \frac{\partial \phi(\eta; p)}{\partial \eta} + \Pr Nt \left[\frac{\partial \theta(\eta; p)}{\partial \eta}\right]^2 + \Pr MEc \left[\frac{\partial f(\eta; p)}{\partial \eta}\right]^2 + \Pr Ec \left[\frac{\partial^2 f(\eta; p)}{\partial \eta^2}\right]^2 \\
& + \Pr Ec \frac{We}{\sqrt{2}} \left[\frac{\partial^2 f(\eta; p)}{\partial \eta^2}\right]^3
\end{aligned} \tag{38}$$

$$\begin{aligned}
\mathcal{N}_\phi\left[f(\eta; p), \theta(\eta; p), \phi(\eta; p)\right] = & \frac{\partial^2 \phi(\eta; p)}{\partial \eta^2} + Lef(\eta; p) \frac{\partial \phi(\eta; p)}{\partial \eta} \\
& + \frac{Nt}{Nb} \frac{\partial^2 \theta(\eta; p)}{\partial \eta^2} - LeCr\phi(\eta; p)
\end{aligned} \tag{39}$$

$$f(0; p) = f_w, \ f'(0; p) = 1 + \Gamma \frac{We}{\sqrt{2}} f''(0 : p), \ f'(\infty; p)$$
$$= 0, \ \theta'(0; p) = -Bi(1 - \theta(\eta; p)), \ \theta(\infty; p)$$
$$= 0, \ \phi'(0; p) = -\frac{Nt}{Nb}\theta'(0; p), \ \phi'(\infty; p) = 0 \tag{40}$$

mth order deformation:

$$\mathcal{L}_f\left[f_m(\eta) - \chi_m f_{m-1}(\eta)\right] = h_f R_{f,m}(\eta) \tag{41}$$

$$\mathcal{L}_\theta\left[\theta_m(\eta) - \chi_m \theta_{m-1}(\eta)\right] = h_\theta R_{\theta,m}(\eta) \tag{42}$$

$$\mathcal{L}_\phi\left[\phi_m(\eta) - \chi_m \phi_{m-1}(\eta)\right] = h_\phi R_{\phi,m}(\eta) \tag{43}$$

where

$$\chi_m = \begin{cases} 0, \ m \le 1 \\ 1, \ m > 1 \end{cases} \tag{44}$$

$$R_{f,m}(\eta) = f'''_{m-1} + \sum_{k=0}^{m-1} We\left(f'''_{m-1-k}f''_k\right) - \sum_{k=0}^{m-1} f_{m-1-k'}f_{k'} + \sum_{k=0}^{m-1} f_{m-1-k}f''_k$$
$$- (M) f_{m-1-k'}\lambda\theta_{m-1}(1 + \beta_t\theta_{m-1}) + \lambda\phi_{m-1}N^*(1 + \beta_c\phi_{m-1}) \tag{45}$$

$$R_{\theta,m}(\eta) = \theta''_{m-1} + Rd((\theta_{m-1}(\theta_w - 1) + 1))^2 \left(3(\theta_w - 1) \sum_{k=0}^{m-1} \theta_{m-1-k'}\theta_{k'} + (\theta_{m-1}(\theta_w - 1) + 1)\theta''_{m-1}\right)$$
$$+ Pr \sum_{k=0}^{m-1} \left[\theta_{m-1-k'}f_k\right]$$
$$- Pr\gamma\left[\left(f_{m-l-1}\sum_{j=0}^{l} f_{1-j'}\theta_{j'} + f_{m-l-1}\theta''_l\right)\right] + PrNb \sum_{k=0}^{m-1} \theta_{m-1-k'}\phi_k + PrNt \sum_{k=0}^{m-1} \theta_{m-1-k'}\theta_{k'} + S\theta_{m-1}$$
$$+ PrEc[f_{m-1-k'}]^2 + PrEc[f''_{m-1-k}]^2 + \frac{1}{\sqrt{2}} PrEcWe[f''_{m-1-k}]^3 \tag{46}$$

$$R_{\phi,m}(\eta) = \phi''_{m-1} + Le \sum_{k=0}^{m-1} \phi_{m-1-k'}f_k + \frac{Nt}{Nb} \sum_{k=0}^{m-1} \theta_{m-1-k'}\theta_{k'} - LeCr\phi_{m-1} \tag{47}$$

$$f_m(0) = 0, \ f_{m'}(0) - \Gamma\frac{We}{\sqrt{2}}f''_m(0) = 0, \ \theta_{m'}(0) - Bi\theta_m(0) = 0, \ \phi_{m'} + \frac{Nt}{Nb}\theta_{m'}(0) = 0$$

$$f_{m'}(\eta) \to 0, \ \theta_{m'}(\eta) \to 0, \ \phi_m(\eta) \to 0 \text{ as } \eta \to \infty. \tag{48}$$

with boundary conditions

$$f_{m'}(0) = f_m(0) = f_{m'}(\infty) = \theta_m(0) = \theta_m(\infty) = \phi_m(0) = \phi_m(\infty) = 0. \tag{49}$$

The appropriate solutions $\left[f_m^*, \theta_m^*, \phi_m^* \right]$ are

$$f_m(\eta) = f_m^*(\eta) + A_1 + A_2 e^{\eta} + A_3 e^{-\eta} \tag{50}$$

$$\theta_m(\eta) = \theta_m^*(\eta) + A_4 e^{\eta} + A_5 e^{-\eta} \tag{51}$$

$$\phi_m(\eta) = \phi_m^*(\eta) + A_6 e^{\eta} + A_7 e^{-\eta} \tag{52}$$

5 Convergence analysis

The above-mentioned HAM algorithm was computed by MATHEMATICA software platform. Significant contributions from the auxiliary constants h_f, h_θ, and h_ϕ were made to the convergence series solutions. Figure 2 shows the h-curves of $f''(0)$, $\theta'(0)$, and $\phi'(0)$. The h-curve, which is a straight line, is noted from these charts. The straight line representing the curves is used to select the convergent approximation. Up to four decimal places, the convergent series solution for the 15th order of approximations is shown in Table 1.
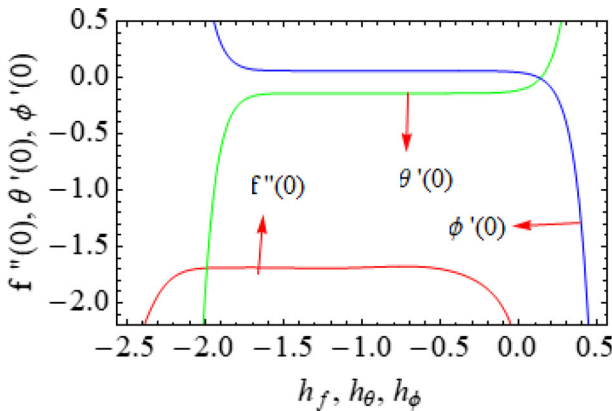
Fig. 2 Curves for h_f, h_θ and h_ϕ.

Table 1 Code justification of $-f''(0)$ for confining case $M = \Gamma = f_w = 0$

Order of approximation	Nadeem [5]	Existing
1	1.04	1.04
5	1.03446	1.03446
10	1.03446	1.03446
15	1.03446	1.03446

6 Computational results and discussion

This section demonstrates the physical justification for velocity, nanomaterial volume percentage, temperature, Bejan impact, and entropy creation rate for a variety of flow parameters. The non-linear ODEs are cracked via HAM.

The impressions of the mass suction/blowing parameter (f_w) on the velocity outline is exposed in Fig. 3a. Figure 3a shows that as the f_w is improved, the velocity profiles drop, thickening the momentum boundary layer. As the dimensionless constant rises, the velocity profile also rises, as shown in Fig. 3b.

Figure 3c illustrates how the fluid flow velocity value grows. The velocity increases as the mixed convection parameter (β_t) value rises. This is because mixed convection happens when the buoyancy of free convection increases significantly. Consequently, the growing mixed convection parameter will result in a growth in buoyancy. Together with the buoyancy force, the flow velocity increases. The velocity graph increases as the ratio of concentration to thermal buoyancy increases, as shown in Fig. 3d. The buoyancy force affects the thermal buoyancy parameter. Stronger buoyancy forces result from larger buoyancy parameters. Such a stronger buoyancy force acts as a catalyst, causing the fluid velocity to rise.

In Fig. 4a, it is depicted that as the θ_w rises, so does the temperature profile. Figure 4b demonstrates that as the quantity of We increases, the temperature curve
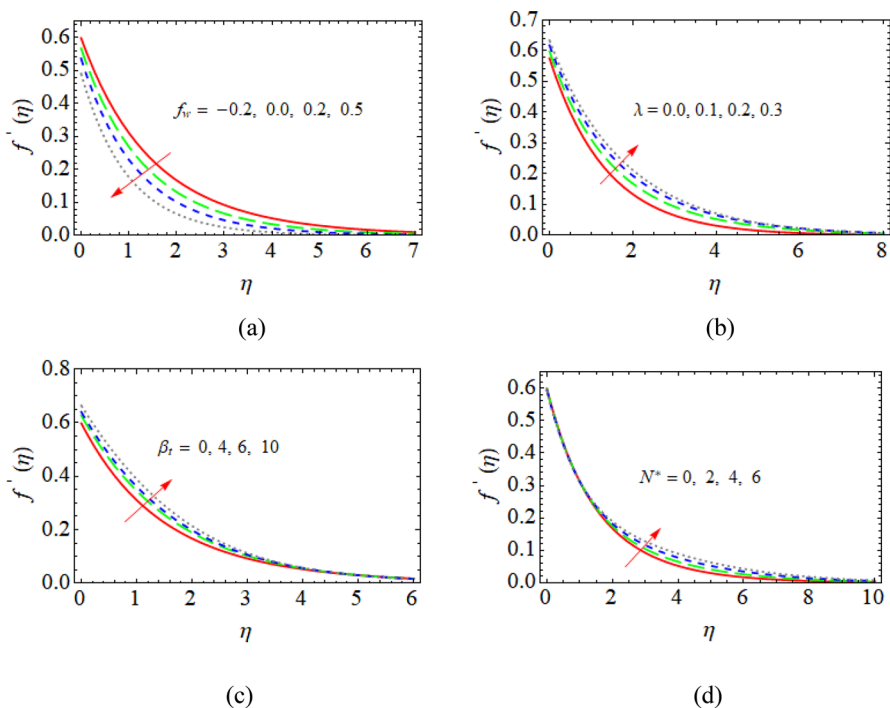

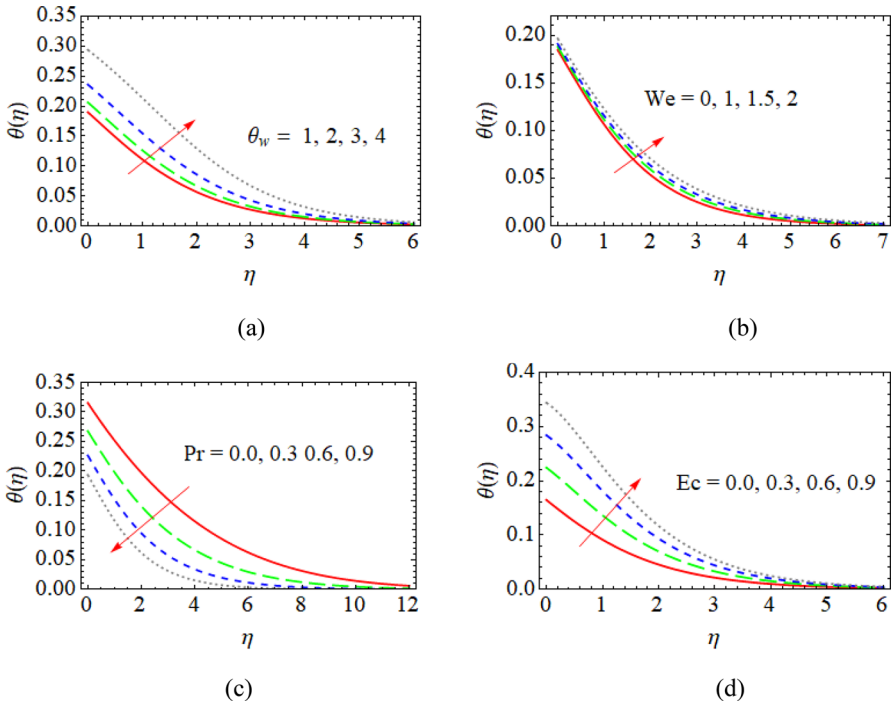**Fig. 3 a–d** Impressions of f_w, λ, ρ_t and N^* on velocity graph

Fig. 4 a–d Impact of θ_w, We, Pr and Ec on temperature profile

and thermal boundary layer both improve. The impression of Prandtl number, Pr, on temperature distribution was shown in Fig. 4c. It is clear that the Prandtl number has a negative connection with the temperature distribution. This is owing to the fact that larger amount of Pr causes the fluid thermal diffusivity to drop, which further causes the thermal boundary layer thickness to decrease.

For Eckert numbers ($Ec = 0.0, 0.3, 0.6, 0.9$), Fig. 4d forecasts Ec impact on the temperature graph, in which we can observe that temperature increases clearly. Ec calculates the energy loss resulting from flow arrangement. Enthalpy variance and the kinetic energy of fluid elements are correlated. We can see from Ec data that the bigger temperature differences are reduced at the sheet's surface. Frictional heating causes the liquid particles to have more kinetic energy than usual. This component caused the thermal boundary layer to expand for a greater Ec.

As seen in Fig. 5a, the fluid concentration falls as Nb upsurges because Brownian motion reasons the boundary layer to warm and cause the elements to leave the fluid regime. On the other hand, the movement of nanoparticles causes thermal conduction to rise with an increase in Nb, and this effect becomes stronger with smaller particles. The fluid concentration rises as the thermophoresis parameter rises, as shown in Fig. 5b. This is because, for smaller values of Pr, thermophoresis heats the boundary layer, slowing the fluid's ability to transmit heat and mass.
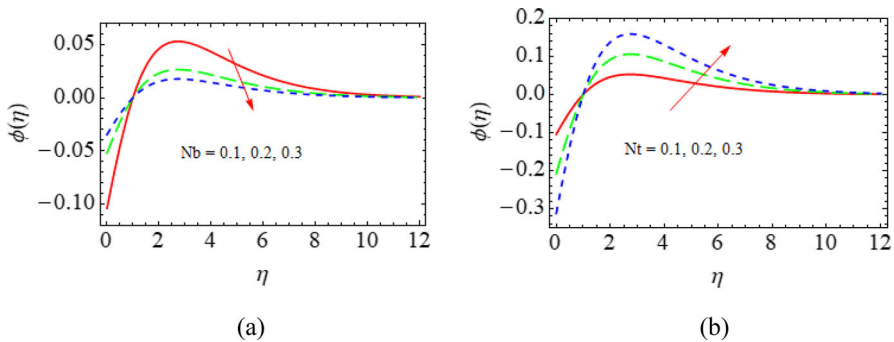
Fig. 5 a, b Impressions of Nt and Nb on Concentration Graph

The impacts of different factors on the entropy generation graph and Bejan number are highlighted in Fig. 6a–h. The relationship between the entropy generation rate and Weissenberg parameter is described in Fig. 6a. Entropy production first appears at the microscopic level when heat transfer increases. Further actions brought by heat transfers cause heat energy to be lost and converted to work. Chaos develops as a result of the additional movement created both inside the structure and outside. Entropy is specifically mentioned as a amount of chaos; "We" is directly inversely related to relaxation time. As a result, fluid particle motion slows down for longer periods of relaxation, which prevents the system's entropy from increasing. As seen in Fig. 6b, the profile of the Bejan number grows as the quantities of the Weissenberg number (We) grow.

The range of the entropy generation initially decreases as Ec increases in Fig. 6c, but it begins to expand as Ec reaches a value of $\eta > 0.4$. According to Fig. 6c and d, the kinetic energy and enthalpy of the boundary layer in the fluid flow physically rise with an rise in the Eckert parameter. As a result, the rate of irreversibility increases. Entropy and Bejan number increase as a result for Eckert number. The impact of the dimensionless constant (λ) on the Bejan number and entropy generation profile is seen in Fig. 6e and f. In Fig. 6e, increasing values of λ cause the range of the Bejan number to initially decrease; but, after it reaches a value of $\eta > 0.6$, it starts to increase. As Fig. 6f illustrates, the dimensionless constant (λ) tends to reduce the Bejan number.

When the Brinkman number rises, the outcome in Fig. 6g and h are inverted. In terms of physics, the Brinkman number predominates the disregarding of heat over viscous heating in comparison to heat transmission in the existence of molecular conduction. Heat transfer by molecular conduction close to the sheet is more efficient at transferring heat than the viscous effect. As a result, a significant amount of heat is produced amid the layers of moving fluid elements. Consequently, the Bejan number dropped and the rate of entropy generation increased.

Figures 7, 8, 9, 10, 11 and 12 show how various fluid parameter effects on skin friction, local heat transfer, and mass transference rates. Figures 7 and 8 show that for the combined settings of We & f_w and We & M, the skin-friction rate decreases. From Fig. 9, it can be seen that the greater radiation impacts is an rise in the rate of heat transference. The outcome of $We\,vs\,Nb$ on the Nusselt and Sherwood numbers
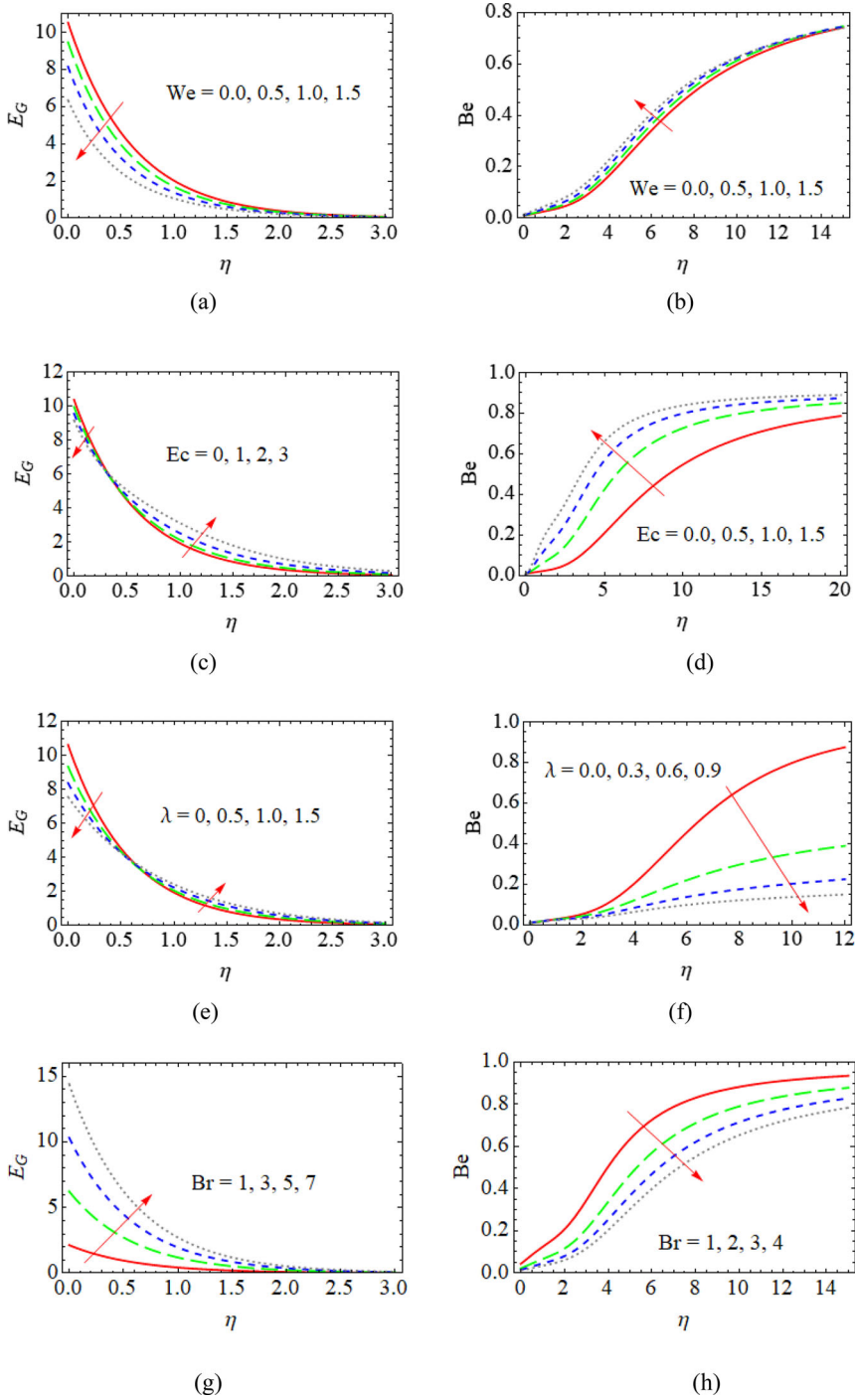
Fig. 6 a–h Impact of We, Ec, λ and Br on Entropy and Bejan number profile

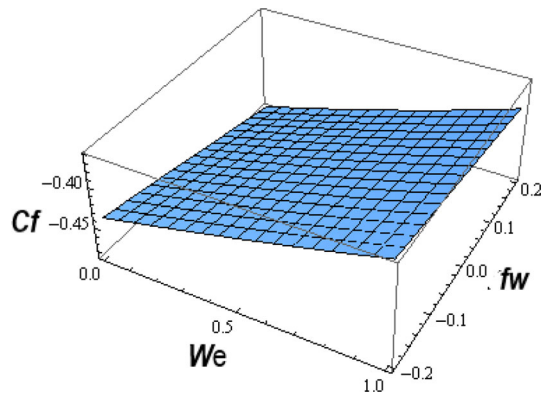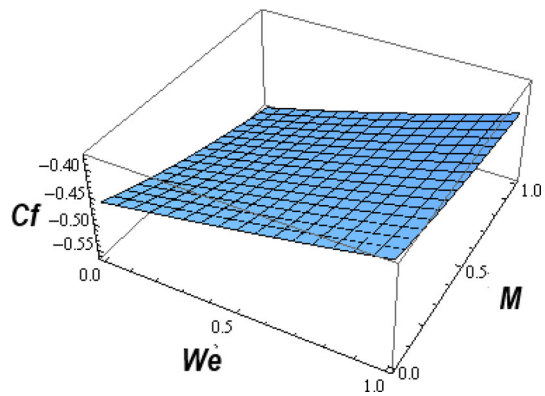**Fig. 7** 3-D plot of $Re^{0.5}Cf$ for $We\&fw$

Fig. 8 3-D plot of $Re^{0.5}Cf$ for $We\&M$

will be examined in Figs. 10 and 11. These charts highlight the declining influence of increasing We values. Additionally, Fig. 10 shows that the Nusselt number quickly decrease as the amount of Nb grow, whereas the amount of the Sherwood number sharply increase with enhancement, as seen in Fig. 11. Positive Nusselt number indicate that heat is being transported physically from a hot object to a cool fluid. Figure 12 displays the mass transference rate for the joint parameters We and Nt. Therefore, we infer from this graph that the mass transference rate decreases as We and Nt increase.

7 Code validation

This section covers code validation of current results. With the exception of the exceptional case $M = K_P = \Gamma = f_w = 0$, a comparative analysis of the order of approximation of HAM for $-f''(0)$ and skin friction $\left(-Re^{0.5}Cf\right)$ is completed by Nadeem et al. [5] (Consult Tables 1 and 2). Early findings of code validation for lower Nusselt number are presented in [29–32]. In Table 3, the validation is displayed. The validation results show a good degree of consistency with previously published findings. As a result, there is maximum confidence in the current simulations.

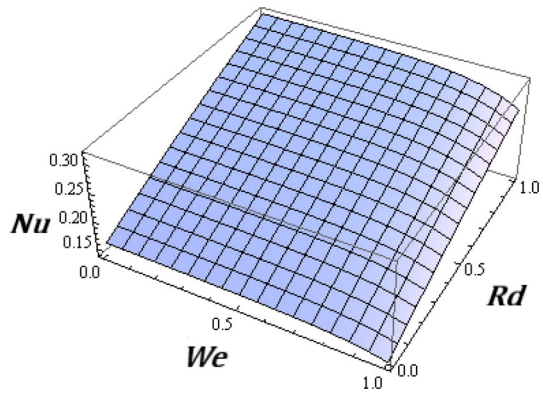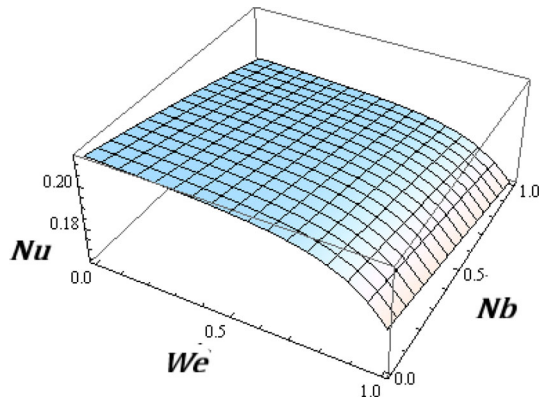**Fig. 9** 3-D plot of $Re^{-0.5}Nu$ for $We\&Rd$

Fig. 10 3-D plot of $Re^{-0.5}Nu$ for $We\&Nb$

8 Final outcomes

In the current study, a stretchable sheet with zero mass flux and Christov-Cattaneo heat flux was used to generate a non-linear mixed convective Williamson nanofluid flow. The governing nonlinear equations are dealt with using the homotopy progress technique. Following discussion of the physical clarification of various physical characteristics related to entropy creation, Bejan number, concentration, velocity, and temperature:

- The velocity graph is increased by the thermal buoyancy parameter and the dimensionless constant, but the suction/blowing parameter exhibits the reverse trend.
- When Eckert number and Weissenberg parameter are strong, the temperature profiles rise.
- The Weissenberg number has an inverse relationship with the range of the heat and mass transfer rate.
- For increased magnetic, suction/injection, and Weissenberg numbers, skin friction rate decreases.
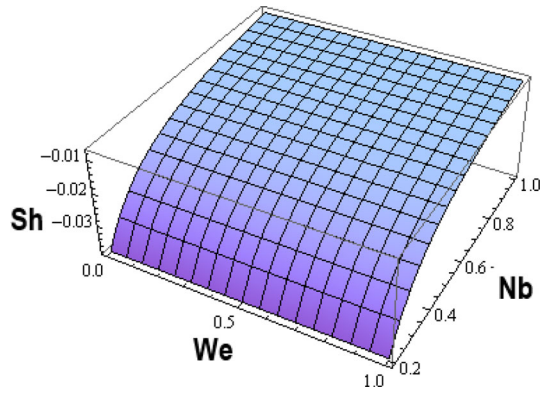
Fig. 11 3-D plot of $Re^{-0.5}Sh$ for $We\&Nb$

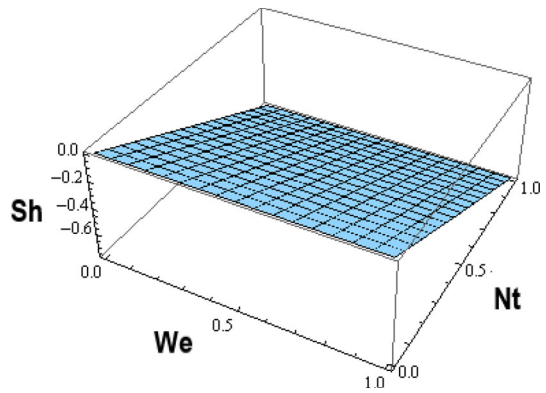
Fig. 12 3-D plot of $Re^{-0.5}Sh$ for $We\&Nt$

Table 2 Code justification of skin-friction $\left(-Re^{0.5}Cf\right)$ for limiting case $M = \Gamma = f_w = 0$

We	Nadeem [5]	Present
0	1	1
0.1	0.97659	0.97659
0.2	0.93982	0.93982
0.3	0.88272	0.88274

Table 3 Evaluation between the specific case with the lowered Nusselt number $Rd = Ec = M = Nt = Nb = We = \gamma = S = \Gamma = f_w = 0$, $Bi \to \infty$

Pr	Wang [29]	Gorla [30]	Khan [31]	Makinde [32]	Present
0.20	0.1691	0.1691	0.1691	0.1691	0.1691
0.70	0.4539	0.5349	0.4539	0.4539	0.4539
2.00	0.9114	0.9114	0.9113	0.9114	0.9114
7.00	1.8954	1.8905	1.8954	1.8954	1.8954

- Thermophoresis and Brownian motion parameters' inverse effects on the mass transfer rate and nanoparticle volume fraction are clearly visible.
- Eckert parameter, dimensionless constant, and Brinkman number all cause a rise in entropy formation, however bigger values of the Weissenberg parameter have the opposite effect.
- It is expected that in the future, several scientific and practical applications will rely on the dynamics of the stream across a stretching plate. The findings of the present study can be applied to various model investigations. The current issue's findings are particularly thrilling in various fields of science and technology, such as microchips, electronic cooling systems, heat exchangers, and more.

Data availability Data available upon request.

Declarations

Conflict of interest The authors declare no conflict of interest.

References

1. Choi, S.: Enhancing thermal conductivity of fluids with nanoparticles. ASME Int. Mech. Eng. Expo. **66**, 99–105 (1995)
2. Kuznetsov, A., Nield, D.: Natural convective boundary-layer flow of a nanofluid past a vertical plate. Int. J. Therm. Sci. **49**, 243–247 (2010)
3. Khan, W., Pop, I.: Boundary-layer flow of a nanofluid past a stretchy sheet. Int. J. Heat Mass Transfer. **53**, 2477–2483 (2010)
4. Haddad, Z., Abu-Nada, E., Oztop, H.F., et al.: Natural convection in nanofluids: are the thermophoresis and Brownian motion effects significant in nanofluid heat transfer enhancement. Int. J. Therm. Sci. **57**, 152–162 (2012)
5. Nadeem, S., Hussain, S.T., Lee, C.: Flow of Williamson fluid over a stretching sheet. Braz. J. Chem. Eng. **30**, 619–625 (2013)
6. Khan, S.U., Rauf, A., Shehzad, S.A., Abbas, Z., Javed, T.: Study of bioconvection flow in Oldroyd-B nanofluid with motile organisms and effective Prandtl approach. Physica A **527**, 121179 (2019)
7. Bilal, S.M., Khan, N.Z., Nisar, R.: FEM simulations to analyze flow and thermal characteristics of Carreau non-Newtonian fluid in a square cavity. Int. J. Emerg. Multidiscipl. Math. (2023). https://doi.org/10.54938/ijemdm.2023.02.1.146
8. Bilal, S., Pan, K., Ullah, A., Anwar, A., Akgül, A.: Aggregation of nanoparticles in flow of Carreau fluid containing gyrotactic microorganisms on extendable cylinder with viscous dissipation aspects by performing numerical simulations. Numer. Heat Transfer Part B Fundamentals (2023). https://doi.org/10.1080/10407790.2023.2287590
9. Fourier, J.B.J.: Theorie Analytique De La Chaleur. Chez Firmin Didot, Paris (1822)
10. Cattaneo, C.: Sulla conduzionedelcalore. Atti del Seminario Matematico e Fisico dell Universita di Modena e Reggio Emilia. **3**, 83–101 (1948)
11. Christov, C.I.: On frame indifferent formulation of the Maxwell-Cattaneo model of finite-speed heat conduction. Mech. Res. Commun. **36**, 481–486 (2009)
12. Loganathan, K., Sivasankaran, S., Bhuvaneswari, M., Rajan, S.: Second-order slip, cross-diffusion and chemical reaction effects on magneto-convection of Oldroyd-B liquid using Cattaneo-Christov heat flux with convective heating. J. Thermal Anal. Calorim. **136**, 401–409 (2019)
13. Imtiaz, M., Alsaedi, A., Shaq, A., Hayat, T.: Impact of chemical reaction on third grade fluid flow with Cattaneo-Christov heat flux. J. Mol. Liq. **229**, 501–507 (2017)
14. Ramadevi, B., Kumar, K.A., Sugunamma, V., et al.: Magnetohydrodynamic mixed convective flow of micropolar fluid past a stretching surface using modified Fourier's heat flux model. J. Therm. Anal. Calorim. (2019). https://doi.org/10.1007/s10973-019-08477-1

15. Rashidi, M.M., Ali, M., Freidoonimehr, N., Nazari, F.: Parametric analysis and optimization of entropy generation in unsteady MHD flow over a stretching rotating disk using artificial neural network and particle swarm optimization algorithm. Energy **55**, 497–510 (2013)

16. Khan, M.I., Alzahrani, F.: Transportation of heat through Cattaneo-Christov heat flux model in non-Newtonian fluid subject to internal resistance of particles. Appl. Math. Mech.-Engl. Ed. **41**, 1157–1166 (2020)

17. López, A., Ibáñez, G., Pantoja, J., Moreira, J., Lastres, O.: Entropy generation analysis of MHD nanofluid flow in a porous vertical microchannel with nonlinear thermal radiation, slip flow and convective-radiative boundary conditions. Int. J. Heat Mass Transfer. **107**, 982–994 (2017)

18. Khan, M.I., Hayat, T., Waqas, M., Khan, M.I., Alsaedi, A.: Entropy generation minimization (EGM) in nonlinear mixed convective flow of nanomaterial with Joule heating and slip condition. J. Mol. Liq. **256**, 108–120 (2018)

19. Qing, J., Bhatti, M.M., Abbas, M.A., Rashidi, M.M., Ali, M.E.S.: Entropy generation on MHD Casson nanofluid flow over a porous stretchy/shrinking surface. Entropy **18**, e18040123 (2016)

20. Sheikholeslami, M., Ganji, D.: Entropy generation of nanofluid in presence of magnetic field using Lattice Boltzmann Method. Physica A **417**, 273–286 (2015)

21. Liao, S., Tan, Y.A.: general approach to obtain series solutions of nonlinear differential. Stud. Appl. Math. **119**(4), 297–354 (2007)

22. Loganathan, K., Rajan, S.: An entropy approach of Williamson nanofluid flow with Joule heating and zero nanoparticle mass flux. J. Therm. Anal. Calorim. **141**, 2599–2612 (2020)

23. Rashidi, M.M., Bagheri, S., Momoniat, E., Freidoonimeh, N.: Entropy analysis of convective MHD flow of third grade non-Newtonian fluid over a stretchy sheet. Ain Shams Eng. J. **8**, 77–85 (2017)

24. Eswaramoorthi, S., Sivasankaran, S., Bhuvaneswari, M., Rajan, S.: Soret and Dufour effects on viscoelastic boundary layer flow over a stretchy surface with convective boundary condition with radiation and chemical reaction. Sci Iran B. **23**(6), 2575–2586 (2016)

25. Aquino, A.I., Ma, L., Bo-ot, T.: Multivalued behavior for a two-level system using Homotopy Analysis Method. Physica A **443**, 358–371 (2016)

26. Chu, Y.M., Nazeer, M., Khan, M.I., Ali, W., Zafar, Z., Kadry, S., Abdelmalek, Z.: Entropy analysis in the Rabinowitsch fluid model through inclined Wavy Channel: constant and variable properties. Int. Commun. Heat Mass Transfer **119**, 104980 (2020)

27. Hayat, T., Shafiq, A., Alsaedi, A.: Effect of joule heating and thermal radiation in flow of third grade fluid over radiative surface. PLoS ONE **9**(1), e83153 (2014)

28. Ghasemi, S.E., Hatami, M., Sarokolaie, A.K., Ganji, D.: Study on blood flow containing nanoparticles through porous arteries in presence of magnetic field using analytical methods. Physica E **70**, 14656 (2015)

29. Wang, C.Y.: Free convection on a vertical stretching surface. ZAMM J. Appl. Math. Mech. **69**, 418–420 (1989)

30. Reddy Gorla, R., Sidawi, I.: Free convection on a vertical stretching surface with suction and blowing. Appl. Sci. Res. **52**, 247–257 (1994)

31. Khan, W.A., Pop, I.: Boundary-layer flow of a nanofluid past a stretching sheet. Int. J. Heat Mass Transf. **53**, 2477–2483 (2010)

32. Makinde, O.D., Aziz, A.: Boundary layer flow of a nanofluid past a stretching sheet with a convective boundary condition. Int. J. Therm. Sci. **50**, 1326–1332 (2011)

33. Gorla, R.S.R., Gireesha, B.J.: Dual solutions for stagnation-point flow convective heat transfer of a Williamson nanofluid past a stretching/shrinking sheet. Heat Mass Trans. **52**, 1153–1162 (2016)